LiqRay: Non-invasive and Fine-grained Liquid Recognition System

Fei Shang, Panlong Yang*, Yubo Yan, Xiang-Yang Li
CAS Key Laboratory of Wireless-Optical Communications, University of Science and Technology of China
shf_1998@outlook.com,{plyang,yuboyan,xiangyangli}@ustc.edu.cn

ABSTRACT

The existing RF-based liquid identification methods commonly require a training network of liquid or the container information, such as material and width. Moreover, status quo methods are inapplicable when the solution height is lower than that of the antenna, which is generally unknown either. This paper proposes *LiqRay*, an RF-based solution, retaining non-invasive and fine-grained liquid recognition abilities, thus can recognize unknown solutions without prior knowledge. In dealing with the unknown container material and width, we utilize a dual-antenna model and craft a relative frequency response factor, exploring diversity of the permittivity in frequency domain. In tackling the unknown heights of solution and antenna, we devise the electric field distribution model at the receiving antenna, solving the unknown heights via spatio-differential model. Among eight different solvents, *LiqRay* can identify alcohol solutions with a concentration difference of 1% with 94.92% accuracy. Nevertheless, *LiqRay* can obtain the relative frequency response factor with a relative error of 6.7% without being affected by the height of the solution. Even if it is merely 4 cm, this is fairly lower than that of most antennas' heights, since the operating frequency is around 2 GHz.

CCS CONCEPTS

• **Human-centered computing** → **Ubiquitous and mobile computing systems and tools**; **Ubiquitous and mobile computing**;

KEYWORDS

Wireless Sensing, Contactless Sensing, Material Identification, Liquid Identification, Complex Permittivity

ACM Reference Format:
Fei Shang, Panlong Yang[1], Yubo Yan, Xiang-Yang Li. 2022. LiqRay: Non-invasive and Fine-grained Liquid Recognition System . In *The 28th Annual International Conference On Mobile Computing And Networking (ACM MobiCom '22), October 17–21, 2022, Sydney, NSW, Australia.* ACM, New York, NY, USA, 14 pages. https://doi.org/10.1145/3495243.3560540

*Corresponding authors

ACM MobiCom '22, October 17–21, 2022, Sydney, NSW, Australia

ACM ISBN 978-1-4503-9181-8/22/10…$15.00
https://doi.org/10.1145/3495243.3560540

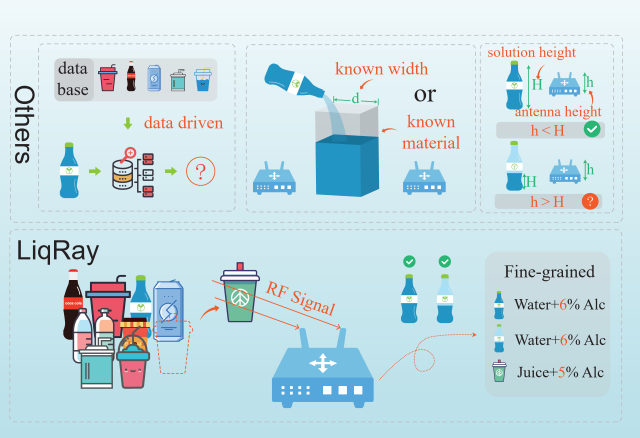

Figure 1: Non-invasive, and fine-grained Liquid recognition system, *LiqRay*.

1 INTRODUCTION

Traditional liquid identification usually relies on the expensive specialized equipments [5, 13, 44, 49]. To facilitate deployment, in recent years, researchers have done a lot of meaningful works based on the communication device, such as RFID and WiFi [14, 15, 23, 48, 63]. Those pioneering studies reduce the deployment cost of the liquid identification systems, whereas there are the following limitations in terms of ease deployment. Tagscan [63], Tagtag [65], WiMi [18] and FG-LiquID [39] propose methods for sensing liquids using RFID, WiFi, or millimeter wave radar. However, they are all data-driven systems, which therefore can't identify unknown solutions that don't exist in the database. It is difficult to build a network with a large amount of training data for recognizing solutions. LiquID [14] and Vi-Liquid [24] build models using UWB and mechanical waves, respectively, to calculate the complex permittivity and viscosity characteristics, which are the object features of the solution. Nonetheless, both of them require prior knowledge of the container (*e.g.* complex permittivity and width) to work. In many case, it is difficult to place a solution into a known container. WiMi [18] implements solution identification independent of container width on WiFi devices. But it can't distinguish concentration at a fine-grained level (For example, identify alcohol solutions with a concentration difference of 1%).

Furthermore, none of these works consider the relative height between the solution and the antenna. However, when the height of the solution is less than that of the antenna, the strength of the received signal correlates with the height of the solution [35, 51, 61]. For example, the WiFi antenna is generally above than 12 cm, but the height of a 400 ml coffee cup is about 8 cm and that of a 330 ml of

Table 1: Comparison of Material Identification Methods with Wireless Signals.

Method	Recognize unknown solutions	Unlimited solution height	Non-invasive		Fine-grained concentration detection(1%)
			No need to know the container material	No need to know the container width	
LiquID[14]	yes	no	no	no	no
Vi-liquid[24]	yes	no	no	yes	no
TagScan[63]	no	no	yes	no	no
Tagtag[65]	no	no	no	yes	no
FG-LiquID[39]	no	no	no	yes	yes
WiMi[18]	no	no	no	yes	no
LiqRay	yes	yes	yes	yes	yes

Coca-Cola is 10.67 cm [1]. Besides, in many cases, we don't even know the height of the solution.

In summary, the aforementioned solutions are absent in the following two design properties:

- *First, non-invasive.* In many cases, the container and the solution require non-invasive measurement, which means that it is not allowed to put the measured liquid into a customized container. As a result, if the system is built based on a container with a specific material and width, it needs to invade the solution to be tested. For non-intrusive liquid recognition, we need to eliminate the effects of container material and width at the same time.
- *Second, fine-grained.* The solutions can be identified on a fine-grained level. For example, using different solvents to dissolve alcohol, we can accurately identify the type of solvent and distinguish the solutions with a concentration difference of 1%.

The basic observation is that different solutions have different complex permittivities, so wireless signals are attenuated differently in different liquids [19, 28, 55]. The *attenuation factor* of the liquid can be applied to construct features for recognizing the solutions. However, there are three challenges needed to be solved first.

(1) First, the attenuation factor cannot be used as a feature to recognize unknown solutions because we cannot get the value of the attenuation factor under non-invasive requirements. In an RF link, the strength of the received signal is affected by the type of solution, the transmission distance in the solution, the distance between the receiving and transmitting antennas, the container material, as well as the antenna gain [19, 27, 28, 35, 59]. Without relying on prior knowledge (such as the container width and material information), it is difficult to eliminate the effects of these factors and get the attenuation factor.

(2) Conventional wireless channel models (*e.g.* CSI model [64]) may require the antenna to be lower than the liquid for liquid recognition. Otherwise, only a portion of the electromagnetic wave reaching the receiving antenna passes through the solution, which makes the strength of the received signal related to the height of the solution. We need to remove the signal difference due to the change in height, but both the antenna's and the solution's height are unknown to us.

(3) The signal has similar attenuation in solutions with similar concentrations, whereas the recognition of fine-grained solutions requires the extraction of discriminative features. For example, after a 2.4 GHz electromagnetic wave transmits 5 cm in two solutions (two alcohol solutions of similar concentrations [7]) with complex permittivity of $75 + 18j$ and $80 + 19j$, the amplitude of the signal is attenuated by 0.78 times and 0.74 times, respectively. This difference is easily drowned out by noise. For the purpose accurately recognizing liquids, we need to use similar signals to construct sufficiently different features.

Solutions. Firstly, based on the attenuation factor, we build an RF-based dual antenna model to eliminate the effects of container material and antenna gain (Sec. 4.1). Notably, the attenuation factor of the solution is related to the signal frequency [7, 8, 36], therefore we extract *the relative frequency response factor* of the solution as the solution feature, which is independent of the container width. Despite the fact that different solutions may have similar attenuation factors at some frequencies [21], due to the different polarization characteristics of molecules, the change trends of the attenuation factors of different solutions are different when the frequency is changed [32, 33]. Taking advantage of the trend in frequency bands, the relative frequency response factor contribute to recognize the solution at a fine-grained level. To facilitate data collection and save frequency band resources, we sample data at four frequency points, that are 1.7 GHz, 2.0 GHz, 2.4 GHz and 2.6 GHz (Sec. 4.3).

Secondly, aimed at eliminating the effect of solution height, we model the transmitting and receiving antennas as thin straight antennas instead of a point. Combined with the distribution of the electric field in space, we extend the model to establish a functional relationship between the received signal strength and the solution height (Sec. 4.4). When the transmitting antenna is displaced a small distance, the electric field below the solution level will change. We extend the dual antenna model so that it can use this difference to extract the relative frequency response factor. In summary, we build a model-driven system to recognize solutions.

Contributions: The major contributions in *LiqRay* is three-fold:

(1) We model the electric field distribution and construct a functional relationship between the received signal strength and the liquid height. Using the electric field difference when the spatial position of the transmitting antenna changes, we extend the model from 2D to 3D, which allows *LiqRay* to recognize the solution independently of the height of the liquid and the antennas.

(2) We build a dual antenna model to eliminate the effect of the container material. Based on the characteristic that the complex permittivity of the solution changes with frequency, we design a

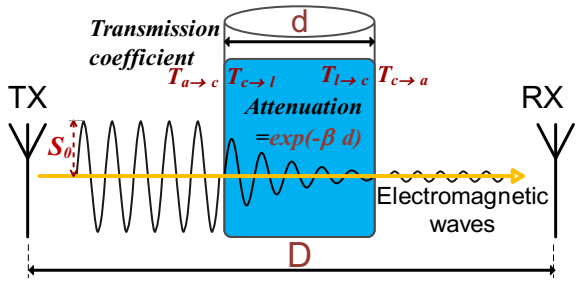

Figure 2: Energy loss of electromagnetic waves: (1) Refraction at the interface of different media; (2)Attenuation in the medium.

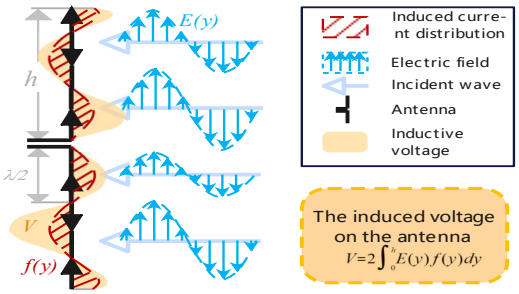

Figure 3: The received signal strength V is the integral of the product of the electric field around the antenna and the induced current.

relative frequency response factor, the relative value of the attenuation factors at multiple frequencies, to eliminate the influence of the container width. Utilizing the relative frequency response factor as a feature, *LiqRay* can recognize the solution independently of the container material and width.

(3) We propose *LiqRay* to identify the concentration and types of alcohol solution in different solvents. Even for similar solvents, such as Coca-Cola and Pepsi, *LiqRay* can identify the alcohol concentration of 1% particle size with an accuracy rate of more than 90%. For solutions with different heights (above 4 cm), *LiqRay* obtains the relative frequency response factor with an average error of 6.7% .

The rest of the paper is organized as follows. In Sec. 2, we present the background of the attenuation factor, RF signal, and antenna. In Sec. 3, we introduce the components of our system. We detail on how to remove the effects of container width and material, the method of recognizing fine-grained solutions, and how to recognize solutions without being affected by the solution height in Sec. 4. In Sec. 5, we make extensive evaluations with several case studies to validate our system. We discuss some practical issues in Sec. 6 and introduce the related work in Sec. 7. Finally, we conclude our work in Sec. 8.

2 PRELIMINARIES

2.1 Attenuation factor of solution

The attenuation factor, is defined as the width of the material needed to decay the strength of the electromagnetic field to $\frac{1}{e}$ of its original value [14, 19]. For ease of representation, we use β to represent the reciprocal of this width, which is given by:

$$\beta = \frac{2\pi}{\lambda_0}\sqrt{\frac{\epsilon'(\sqrt{1+(\frac{\epsilon''}{\epsilon'})^2}-1)}{2}} \tag{1}$$

where λ_0 is the wavelength of electromagnetic waves in the vacuum. ϵ' and ϵ'' are the real and imaginary parts of the complex permittivity of the solution, respectively. The attenuation factor depends merely on the complex permittivity of the solution, which can be used to construct a feature to recognize the solution.

2.2 Signal transmission model

Our signal transmission model is shown in Fig. 2. A container containing the solution is placed in the RF link. When electromagnetic waves are transmitted to the interface of two media (such as air and container wall), they will be refracted and reflected, and part of this energy can be transmitted to the new medium [20, 43, 45]. The fraction of penetrated energy is given by the transmission coefficient, T. In addition, when the signal is transmitted in solution, it will be attenuated. The degree of attenuation is affected by the attenuation factor, β.

As a result, when we send a signal with strength S_0 is sent from TX, the strength of the received signal on RX can be expressed as [14, 29]:

$$S_r = \alpha(D_{air})\Gamma e^{-\beta d} P S_0 \tag{2}$$

where $\alpha(D_{air})$ is the attenuation of electromagnetic waves in air with the transmission distance, d is the transmission distance of signal in liquid, and P is the gain of the receiving antenna. Moreover, Γ is the product of the transmission coefficients across the four interfaces, including two air-container interfaces ($T_{a\to c}$, $T_{c\to a}$) and two container-liquid interfaces ($T_{c\to l}$, $T_{l\to c}$).

The relationship between the complex permittivity and the transmission coefficient, T, is given by [62]:

$$T = \sqrt{\frac{1}{2}\epsilon'(1+\sqrt{1+(\epsilon''/\epsilon')^2})} \tag{3}$$

2.3 The relationship between signal strength and electric field distribution

Since the signal is transmitted differently in the air and solution [6, 26], the height of the solution affects the distribution of the electric field around the receiving antenna, which leads to the difference in the induced voltage on the receiving antenna. To eliminate the influence of height, we need to explore the relationship between the induced voltage and the electric field distribution.

As shown in Fig. 3, a beam of electromagnetic waves incidents the antenna along the negative direction of the x-axis (perpendicular to the antenna) with an electric field whose field strength is $E(y)$. The direction of the electric field is the positive direction of the y-axis (parallel to the antenna). According to the antenna theory [35, 38, 46], it is assumed that the midpoint of the antenna is fed symmetrically by a balanced two-wire transmission line, thus, the length of the antenna is arbitrary, and the current is approximately sinusoidal, which is $f(y)$ in Fig. 3. Therefore, for an antenna with a length of $2h$ that is symmetrical about the midpoint, the total

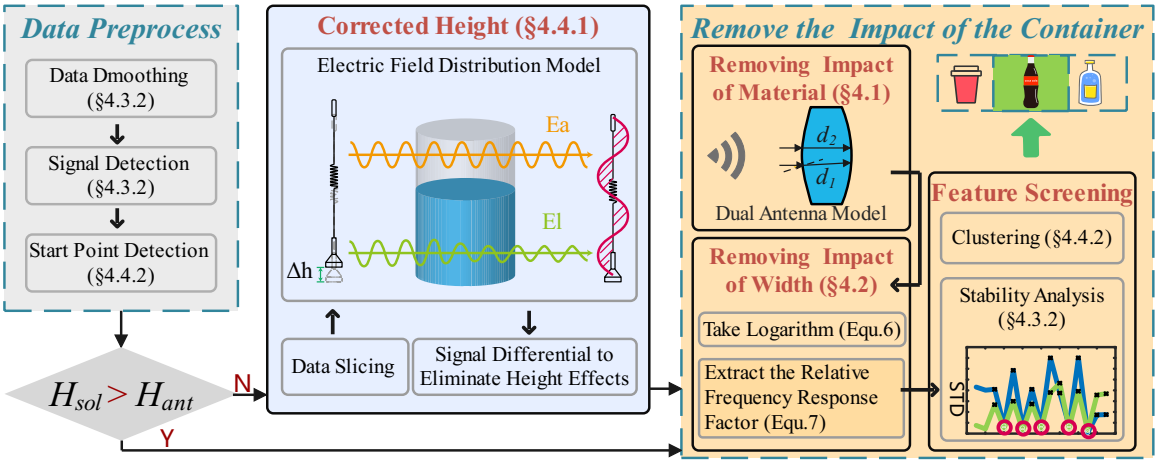

Figure 4: System Overview. Having preprocessed the data, we judge whether the solution is higher than the antenna. If the height of solution (H_{sol}) is less than that of antenna (H_{ant}), we first remove the effect of height. Then we construct the relative frequency response factor that is independent of the width and material of container to recognize the liquids.

induced voltage V is given by:

$$V = 2\int_0^h E(y)f(y)dy \tag{4}$$

3 OVERVIEW

LiqRay consists of three major components: data preprocessing, corrected height, and recognize the solution. We utilize a transmitting antenna and two receiving antennas to construct our system.

Data preprocessing. We process the data collected from the two receiving antennas separately. The data is first filtered and smoothed to suppress noise. Then the Tx movement detection is performed to determine the time when the transmitting antenna starts to rise. Subsequently, a segment of the data is intercepted to recognize the liquid.

Corrected height. We construct an electric field distribution model and control the transmitting antenna to rise a certain distance by a motor. We use the difference of the electric field caused by the displacement of the transmitting antenna to remove the effect of the solution height (Sec. 4.4).

Recognize solution. The intensity of received signal is affected by the material and width of the container, as well as the attenuation factor. We extract the attenuation factor of the solution to construct feature to achieve the purpose of knowing the solution in a fine-grained level. Since the container material has similar effects on the signal strength of the two RF links, we combine the two antenna signals to remove the influence of the container material (Sec. 4.1). Moreover, we take advantage of the different attenuation of signals of different frequencies in the solution to remove the influence of the width of the container (Sec. 4.2). Finally we introduce how the system achieves fine-grained levels in Sec. 4.3.

4 SYSTEM DESIGN

4.1 How to remove the influence of container material and antenna?

Dual antenna model. In order to remove the influence of antenna and container material, we design a dual-antenna model. Figure 5 shows the situation with two receiving antennas. We use one transmitting device to send the signal, and use two antennas on the other device to receive the signal.

For the first RF link, the transmission distance of the signal in the solution is d_1, and the transmission distance of the signal in the air is D_1. Similarly, for the second link, d_2 and D_2 represent the transmission distance of the signal in liquid and air, respectively.

Similar to the Equ. 2, the signal strengths S_{r1} and S_{r2} received by the two receiving antennas are given by:

$$\begin{aligned} S_{r1} &= \alpha(D_1)\Gamma_1 e^{-\beta d_1} P S_0 \\ S_{r2} &= \alpha(D_2)\Gamma_2 e^{-\beta d_2} P S_0 \end{aligned} \tag{5}$$

where $\alpha(.)$ is the attenuation of electromagnetic waves in the air with the transmission distance, and P is the gain of the receiving antenna. The attenuation factor is defined as β and Γ is the product of the transmission coefficients across the four interfaces.

Model analysis. Since the distance between the transmitting and receiving antennas is much larger than the distance between the two receiving antennas, we believe that $D_1 \approx D_2$. In addition, the container and solution that the signal passes through when propagating in the two RF links are the same, the transmission coefficient Γ is also the same. As a result, we can remove the influence of these factors on the signal by simple ratio processing:

$$\Delta S_r = \frac{S_{r1}}{S_{r1}} = e^{-\beta \Delta d} \tag{6}$$

where $\Delta d = d_1 - d_2$.

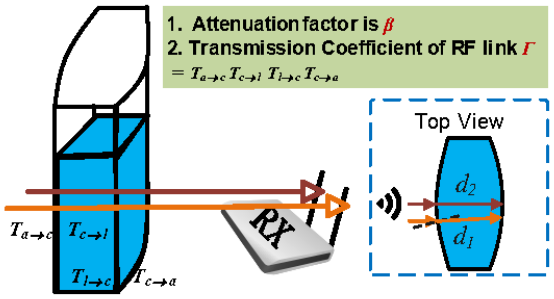

Figure 5: Dual antenna model. The transmission coefficient of the two RF signals is the same.

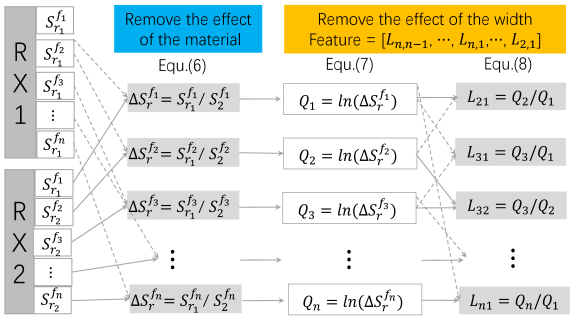

Figure 6: Using the signals of different frequencies to remove the influence of container material and width.

4.2 How to remove the influence of container width?

Based on the fact that the attenuation factor of the solution varies with frequency [21, 37], we extract the relative frequency response of the solution using electromagnetic waves with multiple frequencies, which is independent of the container width.

Challenges in solving attenuation factor. The attenuation factor cannot be solved directly using the received signals without prior knowledge. But in order to non-invasive recognize solutions, the features we design for solutions must contain only attenuation factors. As shown in Equ. 6, the solution factor β and the container width Δd are coupled together. If there are n different RF links in the environment to construct n sets of equations, there are n unknown variables Δd and a solution factor β, totaling n+1 unknown variables. This is an underdetermined system of equations that cannot have an unique solution.

Opportunities brought attenuation factor in different frequency. We note that the attenuation factor β of the signal in the solution is related to the complex permittivity [19, 52]. In addition, the value of the complex permittivity of the solution is related to the frequency of the electromagnetic wave [7, 30, 62]. Therefore, electromagnetic waves with different frequencies will have different degrees of attenuation when passing through the same solution. When the frequency is f_i, we denote the attenuation factor as $\beta(f_i)$. For the same RF link, we transmit signals in m frequencies. Thus, we get m independent equations. Since the position of the antenna does not change, Δd in those m equations is the same. Although still underdetermined, that gives us the possibility to construct solution feature using relative values of attenuation factors, which are independent of transmission distance.

Extracting width-independent relative frequency response factor. In the case that neither the container nor the solution is changed, we collect the signal intensity of electromagnetic waves of different frequencies and form a set $\Delta S_R = [\Delta S_r^{f_1}, \Delta S_r^{f_2}, \ldots, \Delta S_r^{f_n}]$, where f_i is the i-th frequency. When $i \neq j$, we can get:

$$\begin{aligned} Q_i &= \ln(\Delta S_r^{f_i}) = -\beta(f_i)\Delta d_{f_i} \\ Q_j &= \ln(\Delta S_r^{f_j}) = -\beta(f_j)\Delta d_{f_j} \end{aligned} \tag{7}$$

The change of the complex permittivity with frequency results in a change in the transmission coefficient. As a result, the transmission path of the signal in the liquid, Δd, is also a function of frequency. Fortunately, the transmission coefficient varies little with frequency [22]. Figure 7 shows the transmission coefficient's relative variation with frequency of seven common liquids, which is calculated by Equ. 3. The change in the value of the transmission coefficient at 2.6 GHz is less than 0.6% compared to that at 1.7 GHz. And when the position of the antenna and the container are unchanged, the transmission distance of the signal in the liquid is only related to the transmission coefficient. As a result, we believe that Δd is a constant. We can get an equation independent of Δd:

$$L_{i,j} = \frac{Q_i}{Q_j} = \frac{\beta(f_i)}{\beta(f_j)} \tag{8}$$

For i, j changes from 1 to n, we can get the **relative frequency response factor** $F = [L_{n,n-1}, L_{n,n-2}, \ldots, L_{n,1}, L_{n-1,n-2}, \ldots, L_{i,j}, \ldots, L_{2,1}]$. The whole process is shown in Fig.6. [1]

4.3 How to recognize liquids in a fine-grained way?

4.3.1 Build Solution Features. Based on the attenuation factor, we take the relative frequency response as the fingerprint of the solution and use a small amount of frequency band resources to complete the recognizing of the fine-grained solution.

Relative frequency response factor can be used as a fine-grained feature. Figure 8 shows the attenuation factors for 6 different liquids (calculated according to complex permittivities [21] of different frequencies using Equ. 1). It can be found that different liquids have similar attenuation coefficients at some frequencies. Yet the relative frequency response factor constructed based on the attenuation factor is unique. As shown in Equ. 1, the attenuation factor is related to the complex permittivity. Due to the different polarization characteristics of different molecules, the changing trend of the attenuation factor with frequency is different for different solutions [41, 47], which makes the relative frequency response factors can be used to identify solutions at a fine-grained level. We convert the data in Fig. 8 to relative frequency response factors (using Equ. 8), which are shown in Fig. 9. Different solutions have different fingerprint characteristics.

[1] We only need data of three frequencies to construct a fingerprint.

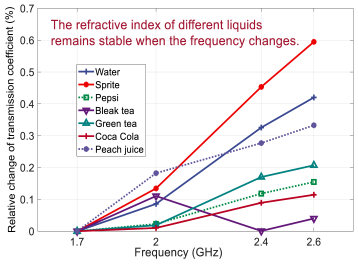

Figure 7: The transmission coefficient remains stable.

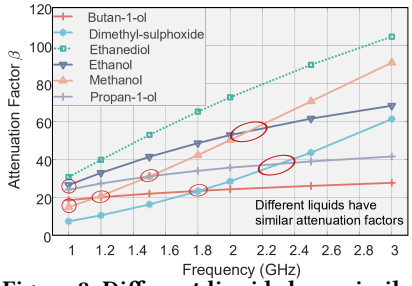

Figure 8: Different liquids have similar attenuation factors at some frequencies.

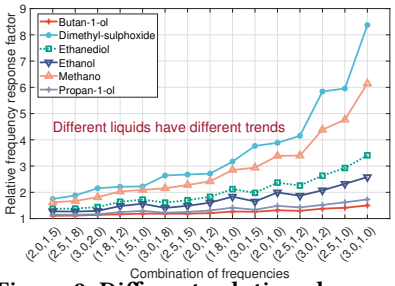

Figure 9: Different solutions have unique relative frequency response factors.

Table 2: Accuracy of recognition under different signals.

Frequency (GHz)	Accuracy rate of concentration recognition	Accuracy rate of species recognition
1.7	65.53%	73.33%
2.0	73.74%	77.93%
2.4	55.38%	63.64%
2.6	70.49%	74.07%
5.0	74.66%	77.12%
1.7,2.0,2.4	83.62%	88.77%
1.7,2.6,5.0	88.71%	90.19%
1.7,2.0, 2.4, 2.6	94.92%	97.30%
1.7,2.0, 2.4, 2.6, 5.0	95.72%	98.93%

We find that some dimensions in Fig. 9 have less dimensional information (such as dimension 1). In order to reduce the time of data collection, we explore the number of frequency points required for recognizing the fine-grained solution with experimental results.

Select the frequencies of the carriers. We use eight common solutions (2.5 L) as solvents, including Water, Sprite, Pepsi, Coca Cola, Master Kong Green Tea, Master Kong Iced Black Tea, Huiyuan Peach Juice, and Huiyuan Orange Juice, in which we dissolve alcohol in concentrations ranging from 0% to 20%, and then recognize them. We use a 3D printed resin container (8 cm×30 cm×30 cm, shown in Fig. 12(b)) to hold the solution. We send 1.7 GHz, 2.0 GHz, 2.4 GHz, 2.6 GHz and 5.0 GHz frequency signals, respectively. Then we use the k-nearest neighbor algorithm (k=1) to recognize the solution. For the single frequency, we use the amplitude ratio of two receiving antennas as the feature (Equ. 6), and for multiple frequencies, we extract the relative frequency response factor as the feature. The results are shown in Table 2. When using the relative frequency response factor as a feature, the recognition accuracy is significantly improved. The same three frequency points are used, and the increase of the frequency interval will increase the accuracy. Considering the small frequency band range of many antennas, we reduce the frequency separation. We find that 4 frequency points can already realize the recognition of the fine-grained solution, and increasing the number of frequency points will not significantly improve the accuracy. Therefore we choose 1.7 GHz, 2.0 GHz, 2.4 GHz and 2.6 GHz to use.

Compared with FG-LiquID[39], which uses 57 GHz to 64 GHz frequency band resources for fine-grained solution identification, we only need to collect signals on some frequency points with an interval greater than 300 MHz.

4.3.2 Data Processing. **Data smoothing and signal extraction.** After the solution is presented in the RF link, the amplitude of the signal is significantly attenuated. When smoothing the amplitude curve, we apply a sliding window to continuously detect if the solution to be tested is present in the RF link. The variance of the amplitude value in sliding window reflects the degree of amplitude fluctuation. When the variance is large and the amplitude decreases, this paper considers a solution to be placed in the RF link; when the variance is large and the amplitude is increasing, we consider a solution to be taken out of the RF link.

Feature Screening. We use electromagnetic waves in four frequency bands (1.7 GHz, 2.0 GHz, 2.4 GHz, and 2.6 GHz). We use water and 5% alcohol as the test solution to collect data 50 times independently. Then we calculate the variance of each dimension feature. We find that feature stability varies widely across dimensions. The main reasons leading to poor data stability are: (1) Interference from other signals, such as WiFi signals in the 2.4G band; (2) $ln(.)$ operations and division operations amplify signal errors. Therefore, we utilize variance to filter the dimensions with stable and use them as the final solution feature.

4.4 How to remove the influence of height?

4.4.1 Height-corrected Model. We find that the solution height affects the strength of the received signal [16], which makes it difficult to obtain stable solution features. In order to eliminate the influence of height, we build a model of the electric field distribution in space and obtain the function relationship between the received signal intensity and the height of the solution. Using the electric field change caused by the displacement of the transmit antenna, we remove the effect of height.

Solution height affects signal strength. For antenna with height of 9 cm, we add water of different heights to a resin container (length, width, and height are 60 cm × 60 cm × 40 cm), and the signal strength on the receiving antenna will also change accordingly. We test the electromagnetic waves of 2.0 GHz, 2.3 GHz and 2.6 GHz respectively, and the results are shown in the Fig. 10(a). When the height of the solution is less than the height of the antenna, the electromagnetic waves of different frequencies are affected to

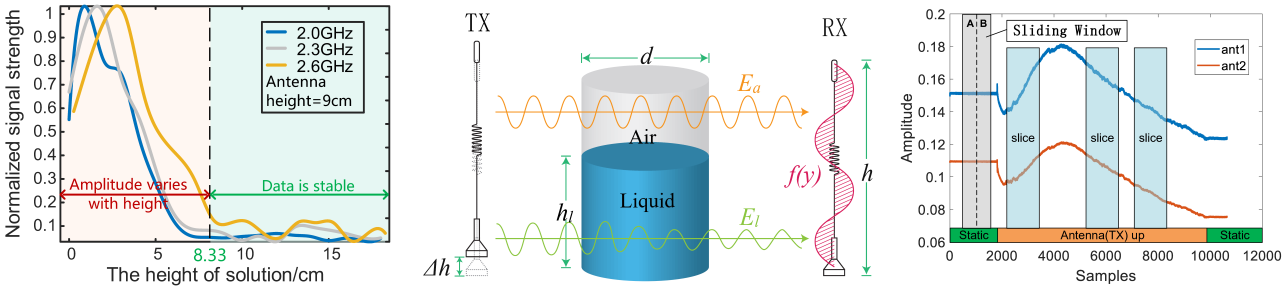

Figure 10: Height-corrected Model. (a) When the liquid height is less than the antenna height, the liquid height will affect the signal strength. (b) When the depth of the solution is less than the height of the antenna, the signal received by the receiving antenna consists of two parts: (1) E_l that reaches the receiving antenna through the liquid; (2) E_a that reaches the receiving antenna through the air. (c) The data collected by the two receiving antennas when the transmitting antenna is slowly raised. We utilize sliding time windows for start point detection and random slices for solution feature extraction.

different degrees, so we cannot design a correction factor in advance to correct the effect of the height.

Electric field distribution model. As shown in Fig. 10(b), the height of the solution is h_l, and the height of the receiving antenna is h. When $h > h_l$, the electromagnetic wave near the receiving antenna is composed of two parts: (1) transmitted from the liquid, the field strength is E_l; (2) transmitted from the air is E_a. When the container is in the far-field region of the transmitting antenna, we treat the incident waves as the plane electromagnetic wave [35]. When sending a signal with a frequency of f, the electric field $\overrightarrow{E_a}$ and $\overrightarrow{E_l}$ are given by:

$$\begin{aligned} \overrightarrow{E_a} &= \Gamma_a \alpha_a \overrightarrow{E_0} \\ \overrightarrow{E_l} &= \Gamma_l \alpha_l \exp(-\beta d) \overrightarrow{E_0} \end{aligned} \tag{9}$$

where d is the transmission distance of a signal in solution, and β is the attenuation factor of the solution. Γ_a and Γ_l are the transmission losses caused by the refraction of the two RF signals during transmission. α_a and α_l are the attenuation of electromagnetic waves. $\overrightarrow{E_a} = E_a \overrightarrow{e_y}$ and $\overrightarrow{E_l} = E_l \overrightarrow{e_y}$, where $\overrightarrow{e_y}$ is the unit vector in the vertical direction.

For the sake of simplicity, we define $\gamma = \frac{T_l \alpha_l}{T_a \alpha_a}$, as a result

$$E_l = \gamma \exp(-\beta d) E_a \tag{10}$$

According to Equ. 4, the signal strength S_r^0 on the antenna is derived by:

$$\begin{aligned} S_r^0 &= \int_0^{h_l} E_l f(y) dy + \int_{h_l}^{h} E_a f(y) dy \\ &= \gamma \exp(-\beta d) E_a \int_0^{h_l} f(y) dy + E_a \int_{h_l}^{h} f(y) dy \end{aligned} \tag{11}$$

where $f(y)$ is the distribution of induced current on the antenna, which is related to the type of antenna and the wavelength of the signal.

Signal differential to eliminate height effects. We collect signals at different h. Every Δh collects the signal strength of the receiving antenna to obtain a sequence $A = [a_0, a_1, \ldots, a_{n-1}]$, where

$$\begin{aligned} a_j = S_r^j &= \int_{j\Delta h}^{h_l} E_l f(y) dy + \int_{h_l}^{h} E_a f(y) dy \\ &= \gamma \exp(-\beta d) E_a \int_{j\Delta h}^{h_l} f(y) dy + E_a \int_{h_l}^{h} f(y) dy \end{aligned} \tag{12}$$

As a result,

$$\begin{aligned} a_{j+1} - a_j &= \gamma \exp(-\beta d) E_a \int_{j\Delta h}^{(j+1)\Delta h} f(y) dy \\ &= \gamma \exp(-\beta d) E_a f(j\Delta h) \Delta h \end{aligned} \tag{13}$$

Two receiving antennas are used in our system, and we compute $\Delta a = a_{j+1} - a_j$ separately on both antennas:

$$\begin{aligned} \Delta a_{rx1} &= \gamma \exp(-\beta d_1) E_a f(j\Delta h) \Delta h \\ \Delta a_{rx2} &= \gamma \exp(-\beta d_2) E_a f(j\Delta h) \Delta h \end{aligned} \tag{14}$$

We calculate their ratio to get:

$$\frac{\Delta a_{rx1}}{\Delta a_{rx2}} = exp(-\beta \Delta d) \tag{15}$$

where $\Delta d = d_1 - d_2$.

Equ. 15 no longer contains height information. We find that Equ. 15 and Equ. 6 have the exact same form. Therefore, we use the method in Sec. 4.2 for subsequent processing to obtain the liquid fingerprint.

4.4.2 Implementation Details. **Tx movement detection.** The signals we collect consist of a three-stage process: the transmitting antenna is stationary; the transmitting antenna is moved upward; and the transmitting antenna is stationary. To recognize the solution, we need to slice the signal collected when the transmitting antenna is raised. As shown in Fig. 10(c), we use the double sliding windows packet detection algorithm to detect the start point of the signal. We set up two fixed-width L and adjacent sliding windows A and B. Later we calculate the variance ratio of signals in the two windows [57]:

$$va_i = \frac{Var(A)}{Var(B)} \tag{16}$$

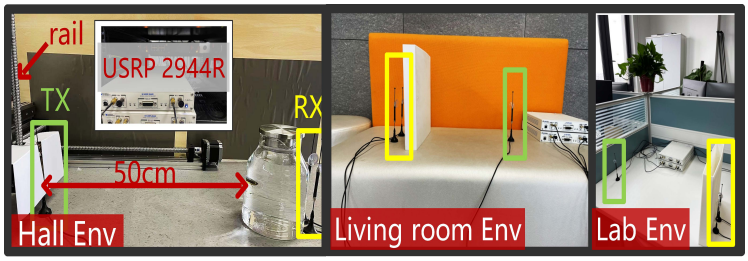

Figure 11: Experimental deployment.

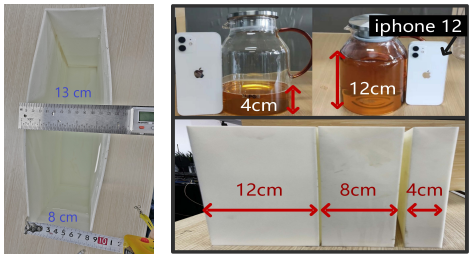

(a) (b)

Figure 12: Experimental container.

where i is the right edge of window A, and the variance of the signal within the window is denoted as $Var(.)$. When both windows contain only the signal in the static, va is small; and when one window contains the signal in the static and the other window contains the signal in the antenna rising, va grows. If the value of va_i is 50 times greater than the value of va_0, we consider that the antenna starts to rise.

Clustering and selecting stable slices. As shown in Equ.13, we only need the data of two adjacent positions to calculate the fingerprint of the solution. However, due to the existence of random noise and other factors, Δa may not be able to perform subsequent processing (such as Δa is a negative value). We devise some methods to avoid that. For each frequency of data, we randomly compute a slice (width is 800 samples). For those slices, we fit a 5th order polynomial to the data and use them to calculate relative attenuation factors. We cluster the attenuation factors for each dimension (choose 0.2 for the inter-class distance) [50]. Then we check if the number of samples in the largest class exceeds 50% of the total. If the number of dimensions satisfying the condition is less than 3, we re-slice the data. Although theoretically the transmitting antenna (TX) only needs a small displacement (Δh) to eliminate the effect of height, due to factors such as random noise and sampling error, this paper raises the TX by at least 2 cmduring the test to ensure enough data to select data slice.

We extend the signal transmission model to remove the effect of height. Using the dual-antenna model and the characteristic that the attenuation factor of the solution changes with frequency, the influence of the material and width of the container is removed, and the purpose of knowing the unknown solution in fine-grained level is achieved.

5 EVALUATION

5.1 Experimental Setup

Hardware setup: As shown in Fig. 11, we use the NI company's N2944R USRP devices to send and receive signals. The antennas can send and receive wireless signals in the frequency range of 698-960 MHz, 1710-2700 MHz and 4900-5850 MHz. We use a computer with Intel i7-10700 CPU and 16 G memory to process the RF data.

Experimental environments: Our experimental setup for evaluating *LiqRay* is shown in Fig. 11. The USRP devices are placed 3 m away from the antennas, and we place containers in the direct path. In the process of collecting data, we continue to send a sine signal at frequencies of 1.7 GHz, 2 GHz, 2.4 GHz, and 2.6 GHz,respectively.

Table 3: Measured Relative attenuation factor with *LiqRay* vs. Ground Truth.

Liquid	Relative attenuation factor			Baseline		
	Fea1	Fea2	Fea3	Fea1	Fea2	Fea3
Water	2.34	1.68	2	2.29	1.62	1.95
Sprite	2.44	1.75	2.05	2.38	1.68	1.99
Pepsi	2.2	1.62	1.9	2.12	1.57	1.83
Coca Cola	2.59	1.77	2.18	2.5	1.71	2.12
Master Kong Iced Black Tea	2.76	1.84	2.29	2.70	1.79	2.23
Master Kong Green Tea	2.91	1.87	2.41	2.81	1.83	2.32
Huiyuan Peach Juice	2.98	1.90	2.46	2.86	1.85	2.37
Huiyuan Orange Juice	2.68	1.79	2.25	2.60	1.76	2.17

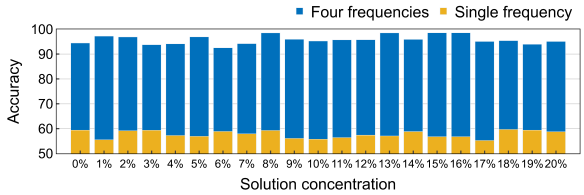

Figure 13: Identification performance of alcohol solutions with different solvents.

5.2 Micro benchmark

Experimental Settings. To verify the effectiveness of our model and techniques, we use eight common solutions as solvents, in which we dissolve alcohol in concentrations ranging from 0% to 20%, and then recognize them. We use a 3D printed resin container (8 cm × 30 cm × 30 cm, which is shown in Fig. 12(a)), to hold the solution. For eight common solutions, we calculate their relative attenuation factors as baselines using their complex permittivities, which are provided by an authoritative Institute of Chemical Technology (Chemical Lab).

Baseline accuracy. As shown in Table 3, the target liquids are common in daily life, including beverages with different formulas, such as Coke and Pepsi. Fea1 is the ratio of attenuation factors at frequencies of 2.6 GHz and 1.7 GHz. Fea2 is the ratio of attenuation factors at frequencies of 2.6 GHz and 2.0 GHz. Fea3 is the ratio of attenuation factors at frequencies of 2.4 GHz and 1.7 GHz.

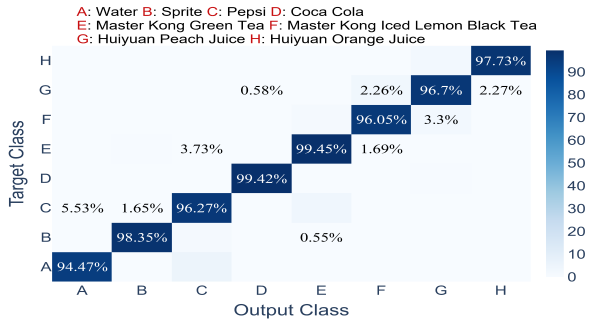

Figure 14: Identification performance for 8 liquids.

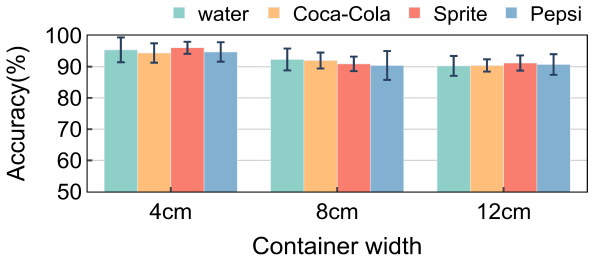

Figure 15: The impact of container width.

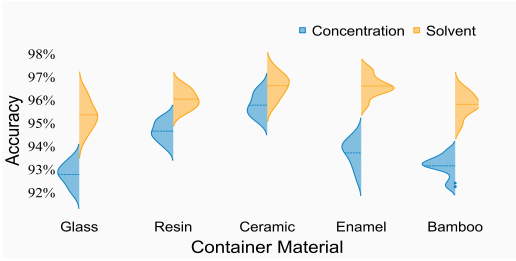

Figure 16: The impact of container material.

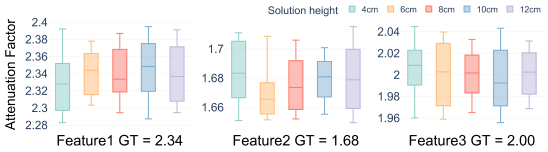

(a) Relative attenuation factor of water at different heights.

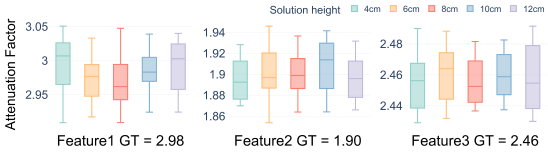

(b) Relative attenuation factor of peach juice at different heights.

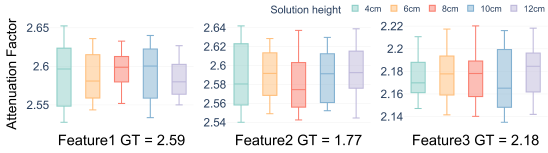

(c) Relative attenuation factor of Coca Cola at different heights.

Figure 17: Solution features remain stable when the height of the solution is changed.

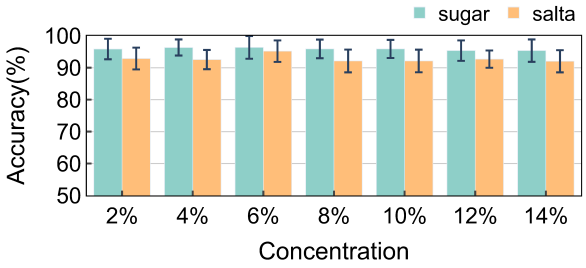

Figure 18: Accuracy in identifying NaCl and sucrose.

Compared with the ground truth, the mean relative error of our system is 4.3% . By taking the relative attenuation factor (using five frequencies) as features, we adopt a simple K-Nearest Neighbors algorithm (K=1) to differentiate those liquids. Fig. 14 presents the resulting confusion matrix, which shows an average classification accuracy of 97.30% . Evidently, *LiqRay* can distinguish a large number of liquids correctly, even if they are highly similar, like Coke and Pepsi.

Recognizing fine-grained solutions. We test eight different solvents: Pepsi, Master Kong Ice Black Tea (a tea beverage), Coca-Cola, Master Kong Green Tea (a tea beverage), Orange juice, Peach juice, water, and Sprite. For each solvent, the alcohol concentration varies from 0 to 20% in 1% steps. For each concentration, we collect data 100 times independently. By taking the relative attenuation factor (using 4 frequencies) as feature, we adopt a simple K-Nearest Neighbors algorithm (K=1) to differentiate those liquids. As shown in Fig. 13, it achieves an average accuracy of 94.92% .

Impact of container material. We pour the target liquids into five different material containers (both have a radius of 5 cm), including glass, resin, ceramic, enamel, and bamboo. The liquids are with different concentrations from 0% to 10% at a step size of 1% and different solvents with Coca-Cola, Sprite, Pepsi, and water. The results are shown in Fig. 16. The average accuracy of concentration identification is 93.54% , and the accuracy of solvent type identification is 95.28% . Containers of different materials have similar accuracy rates.

Impact of container width. The target liquids are poured into containers with three different width (including 4 cm, 8 cm and 12 cm), which are shown in Fig. 12(b). The concentration of liquid is from 0% to 10% at a step size of 1%, 45%, 46% and 78% and different solvents with Coca-Cola, Sprite, Pepsi and water. The results are shown in Fig. 15. In containers of different widths, it can recognize the solution with more than 90% accuracy. However, as the width of the container increases, the attenuation of the signal increases, which reduces the accuracy.

Impact of solution height. We evaluate the impact of the height of the solution on *LiqRay*'s recognition accuracy. We vary the height of the solution to be tested from 4 cm to 12 cm in step of 2 cm. We choose three different liquids including water, Cola, and peach juice. We calculate the features of the same solution when the height of the solution is different, and the results are shown in the Fig. 17. The average error in the relative decay factor is 6.7% when

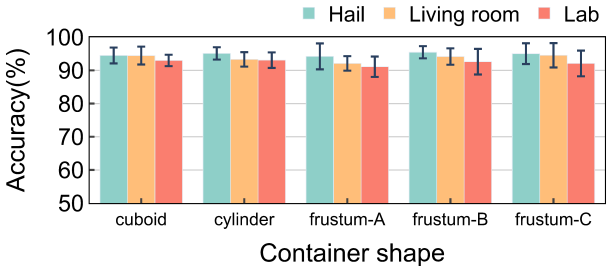

Figure 19: The accuracy of using different shapes containers to hold solutions in different environments.

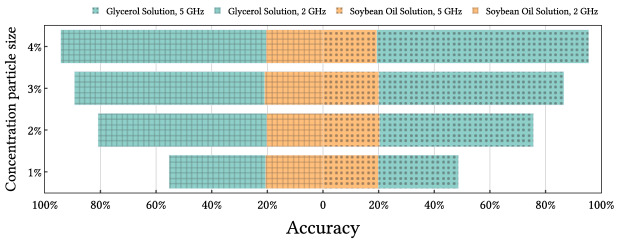

Figure 20: Identification performance of solutions with different oil-based liquids.

the height of the solution changes. This means that our system is still able to recognize the solution when the solution height is different.

5.3 Macro benchmark

***LiqRay*'s performance in different environments with different containers.** As shown in Fig. 11, we test *LiqRay*'s ability to recognize solutions in a hall environment, a simulated living room environment, and a laboratory environment. In each environment, we pour the test liquids into five different shape glass containers, including cube, cylinder, and three irregular shapes. The liquids are with different concentrations from 0% to 10% at a step size of 1%, 45%, 46% and 78% with water. As shown in Fig. 19, containers of different shapes have similar accuracy rates. The difference in accuracy between different containers is less than 4%. and the difference in accuracy between different environments is less than 3%.

***NaCl* and sucrose concentration detection.** Regarding people with high blood pressure and diabetes, controlling salt and sugar intake can help keep them healthy. We perform concentration identification for sodium chloride solutions and sucrose solutions. We dissolve *NaCl* and sucrose in water with a particle size of 2%, and then extract the most characteristic relative attenuation factors, and use the KNN method to recognize them. The results are shown in Fig. 18, and the recognition accuracy is over 93%.

Oil-based concentration detection. We test *LiqRay*'s ability to recognize oil-based liquids using mineral oil as the solvent and soybean oil and glycerol as the solute, respectively. Specifically, we use a resin container of size 30 cm × 30 cm × 8 cm to hold the liquid. We utilize mineral oil as the solvent and soybean oil and glycerol as the solute, respectively. The concentration of the solution is varied from 1% to 20%. For each concentration, data are collected 50 times independently. We use 20% of the data as the test set. Then a KNN (k=1) classifier is used to identify the concentration of the liquid. The results are shown in Fig 20. *LiqRay* can distinguish 2% particle size glycerol solutions with over 78% accuracy. But for the soybean oil solution, *LiqRay* has difficulty distinguishing effectively. We believe the reason is that the attenuation of electromagnetic waves is more pronounced in glycerol than in soybean oil [2, 10, 12]. Since the liquid features depend on the attenuation factor of the liquid, it is difficult to effectively distinguish between lossless media.

6 PRACTICAL ISSUES

6.1 The impact of diffraction

LiqRay is built on the ray tracing model [59]. When the size of the obstacle is similar to the wavelength, the diffraction phenomenon can make the ray tracing model unsuitable [9]. Therefore, we analyze the effect of diffraction by theoretical calculations.

When the container size is large, the effect of diffraction can be ignored. When the length and width of the container exceed 30 cm, the relative error on the results between the Kirchhoff integration [28] and the ray tracing model is less than 1.6%. We believe that the model described in the paper is applicable in this case. Diffraction phenomena can be explained using Huygens' principle [25], and Kirchhoff's integral can be approximated using Huygens' principle [9]. According to Kirchhoff's integral theorem, the field strength of a point P in a closed surface can be regarded as the sum of the effects of each point on the surface on P. As shown in Fig. 21(a), the electromagnetic waves emitted by the point source P' reaches the point P in space through the small hole on the screen. With Kirchhoff approximation [58], Equ. 17 can be written as:

$$E(P) = \frac{ik}{2\pi} \oint_{aperture} \frac{e^{ikR}}{R} \frac{e^{ikR'}}{R'} cos\theta \left(1 + \frac{i}{kR}\right) da \qquad (17)$$

where R and R' are the distances from the element of area da in the aperture to the points P and P', respectively. The angle θ and θ' are those between $\mathbf{R}$ and $\mathbf{n}$, and $\mathbf{R'}$ and $\mathbf{n'}$, respectively. We perform simulation calculations based on Equ. 17 and our experimental setup. Specifically, the distance from the light source P' to the screen of the screen is 0.5 m, and the distance from the observation point to the screen is 1.5 cm. Figure 21(b) shows the difference between the integration results and the ray tracing model. When the container size is larger than 30 cm, the relative difference is less than 1.6%, so we believe that our model can be applied in this case.

For smaller containers in different materials, the KNN classifier can still distinguish different liquids at a fine-grained level despite being affected by diffraction. As shown in Fig. 21(b), when the container size is small (for example, the radius is less than 5 cm), the error of the ray tracing model is large. We use the Mie scattering model [31] to calculate the distribution of the electric field when the solution is different and the container material is different. We find that the difference caused by the change of solution concentration is larger than the change of container material, which

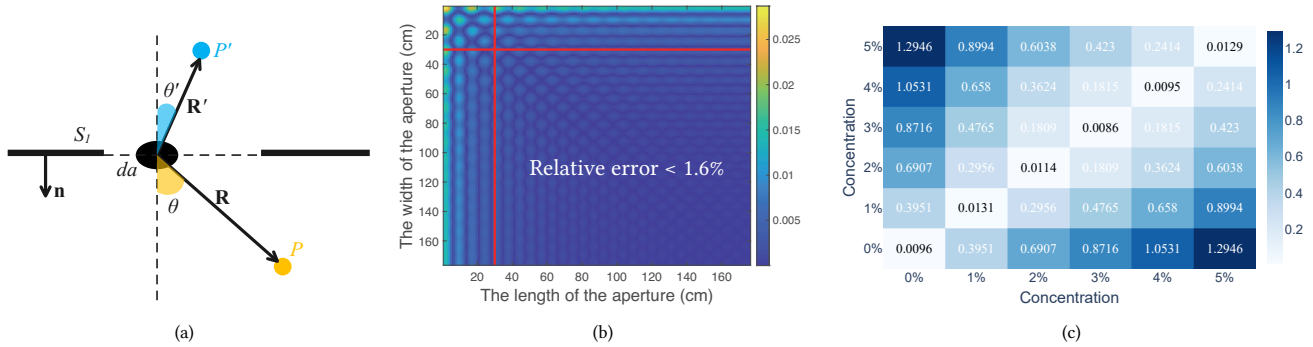

Figure 21: Calculate the effect of diffraction. (a) The electric field intensity at point P is the integral of all secondary light sources on the curved surface S_1; (b) When the container size is greater than 30 cm, the relative error between the calculation results of the ray tracing model and the Kirchhoff integration model is less than 1.6%. (c) The intra-class distance is less than the inter-class distance.

indicates that we can still use the KNN classifier for liquid identification. We use a scattering model [31] to calculate the distribution of electromagnetic fields in space.

We use the Lichtenecker formula [40, 54] to obtain approximate values for different concentrations of alcohol solutions. We set the inner dielectric of the cylinder to an alcohol solution, and the outer dielectric to different materials [3, 11], including wood, glass, hard paper, ceramic, and PVC. We set the width of the container to 5 cm, the thickness of the container to 3 mm, and the angle between the two receiving antennas to be $\pi/6$. We calculate data at frequencies of 1.7 GHz, 2 GHz, 2.4 GHz, and 2.6 GHz. Figure 21(c) shows their intra- and inter-class distance. We find that the difference caused by different materials is smaller than that caused by different concentrations, which indicates that the distinction can be done using the KNN classifier.

6.2 Ability of USRP to distinguish signals

Theoretically, as long as there is a difference in the distance that the signal travels in the liquid, the amplitude of the signal received by the two receiving antennas will be different. However, due to the noise of the receiving device, when the transmission distance is small enough, the receiving device cannot distinguish the two signals. We analyze the difference between the signal amplitudes of the two receiving antennas of *LiqRay*. We explore the limits of USRP's ability to discriminate between signals.

Due to the slight deformation of the container and the rapid attenuation of the signal in the liquid, the amplitude difference between the two receiving antennas is usually more than 8%, which can be distinguished normally by the USRP device. Figure 12(a) shows the container used for the experiment. As shown in Fig. 22(a), we model the two curved sides as a parabola to analyze the difference in the distance that the signal travels in the liquid. Due to the thin walls of the container, when the container is filled with water, it deforms to about 13 cm wide in the middle and about 8 cm wide on the sides. When the distance between the two receiving antennas is 5 cm, the difference between d_1 and d_2 is about 6 mm. For several common beverages (water, Cola, *etc.*), the amplitudes of the signals typically differ by more than 8%.

In addition, we explore the limits of USRP to distinguish signals. For four different frequencies (1.7 GHz, 2 GHz, 2.4 GHz, 2.6 GHz), we independently acquire data 200 times in an empty hall. For each acquired data, we use a Gaussian filter to remove noise. In order to make the signals of different frequencies have the same dimension (the gain of the antenna to the signals of different frequencies is different), we linearly scale the amplitudes of the signals of different frequencies so that their mean is 1. The results are shown in Fig 23. The standard deviation of data collected at different times of the same frequency does not exceed 0.005. Therefore, we believe that the difference between the signals that can be distinguished by USRP should be no less than 1%. For a 2 GHz signal, the transmission distance of the signal in water is greater than 1.6 mm, and when the frequency rises to 5 GHz, this threshold is reduced to 0.6 mm.

6.3 Antenna coupling

In deployment, the distance between two receiving antennas may be less than half a wavelength. Antenna coupling affects the amplitude of the received signal because the mutual impedance among multiple antennas affects the equivalent impedance of the receiving antenna [34]. In this case, the mutual coupling of the antennas may affect the strength of the received signal. We use the ENA vector network analyzer (KEYSIGHT E5071C) to test the change of the reflection coefficient of the antenna when the distance between the two receiving antennas is different, and the results are shown in the Fig. 24. Compared with 10 cm, when the antenna spacing is 4 cm, the change of the reflection coefficient does not exceed 0.4 dB, which indicates that the change of the received signal amplitude does not exceed 2%. The diameter of the antenna used for liquid identification is 3 cm and the distance between the antennas is more than 4 cm, so we believe that the antenna coupling does not affect the amplitude of the received signal.

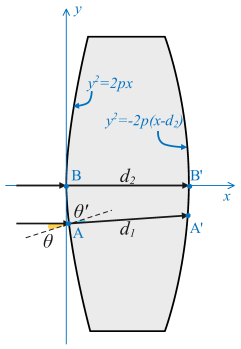

Figure 22: The deformed container.

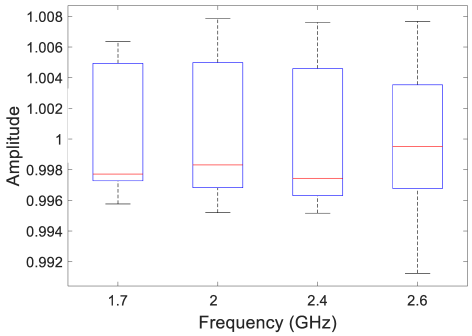

Figure 23: The standard deviation of repeated collection data is less than 0.005.

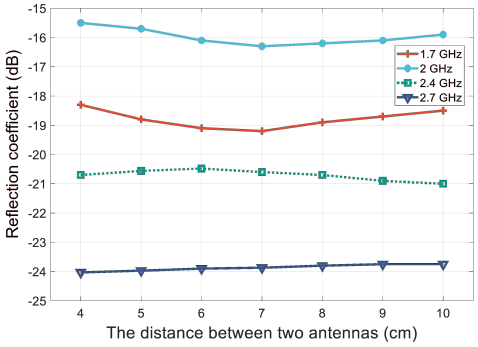

Figure 24: The reflection coefficient are relatively stable across different distances.

7 RELATED WORK

RF-based liquid detection method. Recently, in the field of liquid identification, researchers have proposed many excellent systems based on RF [14, 23, 48, 63]. Those methods can be divided into two categories, one is data-driven, which requires pre-trained features to distinguish different liquids; the other is model-driven, which builds models to obtain the physical or chemical parameters of the liquid itself (such as complex permittivity).

(1) *Data-driven method.* Tagscan [63] extracts the RSSI and phase change as features from RFID tag reading to create a database and classify 10 liquids. Tagtag [65] propose to attach one RFID tag on the target of interest for liquid testing, which can detect fake alcohol, baby formula adulteration, fake luxury CHANEL perfume, and expired milk by comparing with the training set. FG-LiquID [39] designs a novel neural network for sensing liquids using millimeter wave radar, which can identify 30 different liquids in a fine-grained manner. In addition to not being able to identify the unknown liquids, it is inconvenient to build a database containing lots of kinds of solutions. Therefore, we use a model-driven approach to construct the system with the attenuation factor.

(2) *Model-driven method.* LiquID [14] uses the amplitude and phase of the signal to solve the equation to obtain the complex permittivity of the liquid, which is able to identify 33 kinds of liquids. Using mechanical waves, Vi-Liquid [24] builds a model to compute the viscosity of the liquid, which realizes the identification of 30 kinds of liquids. But these methods usually rely on prior knowledge, such as the material and width of the container. Having built a dual-antenna model and extracted the relative frequency response factor as a feature of the liquid, we construct a container-independent system.

They only identify liquids in the 2D ranges without considering the relative height of the solution to the antenna. We construct the distribution model of the electric field and eliminate the influence of height by using the change of the electric field when the transmitting antenna is displaced and completed the solution recognition in the 3D range.

Traditional liquid identification methods. Traditionally, material recognition requires the use of expensive specialized equipment to provide data [4, 17, 53, 56, 60]. In addition to expensive equipment, these methods typically require immersing the probe in a solution to collect the signal and further analyze the spectral information with a spectrometer.

Optical and camera based liquid detection method. Recent research on optical and camera-based liquid detection method has many different problem-solving theories and meaningful applications [23, 42, 48, 66]. Smart-U [23] can recognize food or liquid in the spoon by employing the LEDs and photodiodes. However, these methods are not easy to deploy in daily life. CapCam [66] uses the phone's camera to capture the ripples created by vibrations in the solution to recognize the solution. But it only recognizes clear solutions.

8 CONCLUSION

This paper presents *LiqRay*, a non-invasive and fine-grained system that can use RF signals to recognize unknown solutions. We develop a new computational model independent of the container material and width, as well as the solution height, which allows us to recognize unknown solutions in unknown containers. Our comprehensive experiments show that *LiqRay* can discriminate between alcoholic solutions with a concentration difference of 1%, monitoring sugar and salt intake. It can cope with different containers and solution heights. Our model-driven scheme is making efforts to cultivate liquid recognition system pervasive and robust enough for more applications and scenarios.

ACKNOWLEDGMENTS

The research is partially supported by NSFC with No. 62072424, U20A20181, the University Synergy Innovation Program of Anhui Province with No. GXXT-2019-024, National Key R&D Program of China 2018YFB0803400, National Key R&D Program of China under Grant No. 2021ZD0110400, China.National Natural Science Foundation with No. 62132018, Key Research Program of Frontier Sciences, CAS. No. QYZDY-SSW-JSC002.

REFERENCES

[1] Amazon. [n. d.]. COCA COLA CANS 330ML PK24 A00768 VRBCOKE. [EB/OL]. https://www.amazon.com/COCA-COLA-330ML-A00768-VRBCOKE/dp/B0051GNHJ4.

[2] R Behrends, K Fuchs, U Kaatze, Y Hayashi, and Y Feldman. 2006. Dielectric properties of glycerol/water mixtures at temperatures between 10 and 50 C. *The Journal of chemical physics* 124, 14 (2006), 144512.

[3] Mohammed Bendaoued, Jaouad Terhzaz, and Rachid Mandry. 2017. Determining the complex permittivity of building dielectric materials using a propagation constant measurement. *International Journal of Electrical and Computer Engineering* 7, 4 (2017), 1681.

[4] CR Blakley, JJ Carmody, and ML Vestal. 1980. Liquid chromatograph-mass spectrometer for analysis of nonvolatile samples. *Analytical Chemistry* 52, 11 (1980), 1636–1641.

[5] C Blom and J Mellema. 1984. Torsion pendula with electromagnetic drive and detection system for measuring the complex shear modulus of liquids in the frequency range 80–2500 Hz. *Rheologica acta* 23, 1 (1984), 98–105.

[6] PP Bobrov, AS Lapina, and AV Repin. 2015. Effect of the rock/water/air interaction on the complex dielectric permittivity and electromagnetic waves attenuation in water-saturated sandstones. In *PIERS Proceedings*. 1877–1879.

[7] Xavier Bohigas and Javier Tejada. 2010. Dielectric characterization of alcoholic beverages and solutions of ethanol in water under microwave radiation in the 1–20 GHz range. *Food research international* 43, 6 (2010), 1607–1613.

[8] Roland Böhmer, M Maglione, Peter Lunkenheimer, and Alois Loidl. 1989. Radio-frequency dielectric measurements at temperatures from 10 to 450 K. *Journal of applied physics* 65, 3 (1989), 901–904.

[9] Max Born and Emil Wolf. 2013. *Principles of optics: electromagnetic theory of propagation, interference and diffraction of light*. Elsevier.

[10] MM Brady and SS Stuchly. 1981. Dielectric dispersion of glycerol from 2.0 to 4.0 GHz. *The Journal of Chemical Physics* 74, 6 (1981), 3632–3633.

[11] Amir Čenanović, Siegfried Martius, Andreas Kilian, Jan Schür, and Lorenz-Peter Schmidt. 2011. Non destructive complex permittivity determination of glass material with planar and convex surface. In *2011 German Microwave Conference*. IEEE, 1–4.

[12] Julián Corach, Eriel Fernández Galván, Patricio Aníbal Sorichetti, and Silvia Daniela Romano. 2019. Estimation of the composition of soybean biodiesel/soybean oil blends from permittivity measurements. *Fuel* 235 (2019), 1309–1315.

[13] Juan de Vicente, Modesto T López-López, Juan DG Durán, and Fernando González-Caballero. 2004. Shear flow behavior of confined magnetorheological fluids at low magnetic field strengths. *Rheologica acta* 44, 1 (2004), 94–103.

[14] Ashutosh Dhekne, Mahanth Gowda, Yixuan Zhao, Haitham Hassanieh, and Romit Roy Choudhury. 2018. Liquid: A wireless liquid identifier. In *Proceedings of the 16th Annual International Conference on Mobile Systems, Applications, and Services*. 442–454.

[15] Paola Donato, Francesco Cacciola, Peter Quinto Tranchida, Paola Dugo, and Luigi Mondello. 2012. Mass spectrometry detection in comprehensive liquid chromatography: basic concepts, instrumental aspects, applications and trends. *Mass spectrometry reviews* 31, 5 (2012), 523–559.

[16] Vicko Doric, Dragan Poljak, John Paul, and Christos Christopoulos. 2007. Modeling of a straight thin wire: comparison of antenna approach and transmission line model. In *2007 15th International Conference on Software, Telecommunications and Computer Networks*. IEEE, 1–3.

[17] John F Federici. 2012. Review of moisture and liquid detection and mapping using terahertz imaging. *Journal of Infrared, Millimeter, and Terahertz Waves* 33, 2 (2012), 97–126.

[18] Chao Feng, Jie Xiong, Liqiong Chang, Ju Wang, Xiaojiang Chen, Dingyi Fang, and Zhanyong Tang. 2019. WiMi: Target material identification with commodity Wi-Fi devices. In *2019 IEEE 39th International Conference on Distributed Computing Systems (ICDCS)*. IEEE, 700–710.

[19] Richard P Feynman, Robert B Leighton, and Matthew Sands. 2011. *The Feynman lectures on physics, Vol. I: The new millennium edition: mainly mechanics, radiation, and heat*. Vol. 1. Basic books.

[20] Daniel Fleisch. 2008. *A student's guide to Maxwell's equations*. Cambridge University Press.

[21] Andrew P Gregory and RN Clarke. 2012. Tables of the complex permittivity of dielectric reference liquids at frequencies up to 5 GHz. (2012).

[22] David J Griffiths. 2005. Introduction to electrodynamics.

[23] Qianyi Huang, Zhice Yang, and Qian Zhang. 2018. Smart-U: smart utensils know what you eat. In *IEEE INFOCOM 2018-IEEE Conference on Computer Communications*. IEEE, 1439–1447.

[24] Yongzhi Huang, Kaixin Chen, Yandao Huang, Lu Wang, and Kaishun Wu. 2021. Vi-liquid: unknown liquid identification with your smartphone vibration.. In *MobiCom*. 174–187.

[25] Christiaan Huygens. 1920. *Traité de la lumière*. Gauthier-Villars.

[26] Akira Ishimaru. 2017. *Electromagnetic wave propagation, radiation, and scattering: from fundamentals to applications*. John Wiley & Sons.

[27] Aravind Iyer, Catherine Rosenberg, and Aditya Karnik. 2009. What is the right model for wireless channel interference? *IEEE Transactions on Wireless Communications* 8, 5 (2009), 2662–2671.

[28] John David Jackson. 1999. Classical electrodynamics.

[29] Shan Jiang and Stavros Georgakopoulos. 2011. Electromagnetic wave propagation into fresh water. *Journal of Electromagnetic Analysis and Applications* 2011 (2011).

[30] Udo Kaatze. 1989. Complex permittivity of water as a function of frequency and temperature. *Journal of Chemical and Engineering Data* 34, 4 (1989), 371–374.

[31] M Kerker and E Matijević. 1961. Scattering of electromagnetic waves from concentric infinite cylinders. *JOSA* 51, 5 (1961), 506–508.

[32] John G Kirkwood. 1936. On the theory of dielectric polarization. *The Journal of Chemical Physics* 4, 9 (1936), 592–601.

[33] John G Kirkwood. 1939. The dielectric polarization of polar liquids. *The Journal of Chemical Physics* 7, 10 (1939), 911–919.

[34] J. D. Kraus and R. J. Marhefka. 2003. *Antennas for all applications*. Antennas for all applications.

[35] John D Kraus and Ronald J Marhefka. 2011. Antenna: For all applications (Third Editions)[M]. *Beijing, Publishing House Of Electronics Industry* (2011).

[36] Jerzy Krupka. 2006. Frequency domain complex permittivity measurements at microwave frequencies. *Measurement Science and Technology* 17, 6 (2006), R55.

[37] Jerzy Krupka. 2006. Frequency domain complex permittivity measurements at microwave frequencies. *Measurement Science and Technology* 17, 6 (apr 2006), R55–R70. https://doi.org/10.1088/0957-0233/17/6/r01

[38] Youbok Lee et al. 2003. Antenna circuit design for RFID applications. *AN710, Microchip Technology Inc* (2003).

[39] Yumeng Liang, Anfu Zhou, Huanhuan Zhang, Xinzhe Wen, and Huadong Ma. 2021. FG-LiquID: A Contact-Less Fine-Grained Liquid Identifier by Pushing the Limits of Millimeter-Wave Sensing. *Proc. ACM Interact. Mob. Wearable Ubiquitous Technol.* 5, 3, Article 116 (sep 2021), 27 pages. https://doi.org/10.1145/3478075

[40] Karl Lichtenecker. 1926. Die dielektrizitatskonstante naturlicher und kunstlicher mischkorper. *Physikalische Zeitschrift* 27 (1926), 115–158.

[41] Hans J Liebe, George A Hufford, and Takeshi Manabe. 1991. A model for the complex permittivity of water at frequencies below 1 THz. *International Journal of Infrared and Millimeter Waves* 12, 7 (1991), 659–675.

[42] Hidenori Matsui, Takahiro Hashizume, and Koji Yatani. 2018. Al-light: An alcohol-sensing smart ice cube. *Proceedings of the ACM on Interactive, Mobile, Wearable and Ubiquitous Technologies* 2, 3 (2018), 1–20.

[43] Igor S Nefedov, Ari J Viitanen, and Sergei A Tretyakov. 2005. Electromagnetic wave refraction at an interface of a double wire medium. *Physical Review B* 72, 24 (2005), 245113.

[44] Agilent Application Note. 2006. Agilent basics of measuring the dielectric properties of materials. *Agilent literature number* (2006), 1–34.

[45] Charles Herach Papas. 2014. *Theory of electromagnetic wave propagation*. Courier Corporation.

[46] Dragan Poljak, Sinisa Antonijevic, Khalil El Khamlichi Drissi, and Kamal Kerroum. 2010. Transient response of straight thin wires located at different heights above a ground plane using antenna theory and transmission line approach. *IEEE transactions on electromagnetic compatibility* 52, 1 (2010), 108–116.

[47] Bin Quan, Xiaohui Liang, Guangbin Ji, Yan Cheng, Wei Liu, Jianna Ma, Yanan Zhang, Daoran Li, and Guoyue Xu. 2017. Dielectric polarization in electromagnetic wave absorption: review and perspective. *Journal of Alloys and Compounds* 728 (2017), 1065–1075.

[48] Tauhidur Rahman, Alexander T Adams, Perry Schein, Aadhar Jain, David Erickson, and Tanzeem Choudhury. 2016. Nutrilyzer: A mobile system for characterizing liquid food with photoacoustic effect. In *Proceedings of the 14th ACM Conference on Embedded Network Sensor Systems CD-ROM*. 123–136.

[49] Christian Riesch, Erwin K Reichel, Franz Keplinger, and Bernhard Jakoby. 2008. Characterizing vibrating cantilevers for liquid viscosity and density sensing. *Journal of sensors* 2008 (2008).

[50] Lior Rokach and Oded Maimon. 2005. Clustering methods. In *Data mining and knowledge discovery handbook*. Springer, 321–352.

[51] A Salinas, R Gomez Martin, A Rubio Bretones, and I Sanchez Garcia. 1994. Modelling of straight thin wires using time-domain electric field integral equations. *IEE Proceedings-Microwaves, Antennas and Propagation* 141, 2 (1994), 123–126.

[52] Andrew Shaw, AI Al-Shamma'a, SR Wylie, and D Toal. 2006. Experimental investigations of electromagnetic wave propagation in seawater. In *2006 european microwave conference*. IEEE, 572–575.

[53] Chenjun Shi, Ji Zhu, Mingqian Xu, Xu Wu, and Yan Peng. 2020. An Approach of Spectra Standardization and Qualitative Identification for Biomedical Materials Based on Terahertz Spectroscopy. *Scientific Programming* 2020 (2020).

[54] Ray Simpkin. 2010. Derivation of Lichtenecker's logarithmic mixture formula from Maxwell's equations. *IEEE Transactions on Microwave Theory and Techniques* 58, 3 (2010), 545–550.

[55] F Stern and C Weaver. 1970. Dispersion of dielectric permittivity due to space-charge polarization. *Journal of Physics C: Solid State Physics* 3, 8 (1970), 1736.

[56] Monika Szymańska-Chargot, Justyna Cybulska, and Artur Zdunek. 2011. Sensing the structural differences in cellulose from apple and bacterial cell wall materials by Raman and FT-IR spectroscopy. *Sensors* 11, 6 (2011), 5543–5560.

[57] John Terry and Juha Heiskala. 2002. *OFDM wireless LANs: A theoretical and practical guide*. Sams publishing.

[58] Eric I Thorsos. 1988. The validity of the Kirchhoff approximation for rough surface scattering using a Gaussian roughness spectrum. *The Journal of the*

Acoustical Society of America 83, 1 (1988), 78–92.

[59] David Tse and Pramod Viswanath. 2005. *Fundamentals of wireless communication*. Cambridge university press.

[60] Georgios Tsiminis, Fenghong Chu, Stephen C Warren-Smith, Nigel A Spooner, and Tanya M Monro. 2013. Identification and quantification of explosives in nanolitre solution volumes by Raman spectroscopy in suspended core optical fibers. *Sensors* 13, 10 (2013), 13163–13177.

[61] Martin A Uman, D Kenneth McLain, and E Philip Krider. 1975. The electromagnetic radiation from a finite antenna. *American Journal of Physics* 43, 1 (1975), 33–38.

[62] Hippel AR Von and R Arthur. 1954. Dielectrics and waves.

[63] Ju Wang, Jie Xiong, Xiaojiang Chen, Hongbo Jiang, Rajesh Krishna Balan, and Dingyi Fang. 2017. TagScan: Simultaneous target imaging and material identification with commodity RFID devices. In *Proceedings of the 23rd Annual International Conference on Mobile Computing and Networking*. 288–300.

[64] Dan Wu, Daqing Zhang, Chenren Xu, Hao Wang, and Xiang Li. 2017. Device-free WiFi human sensing: From pattern-based to model-based approaches. *IEEE Communications Magazine* 55, 10 (2017), 91–97.

[65] Binbin Xie, Jie Xiong, Xiaojiang Chen, Eugene Chai, Liyao Li, Zhanyong Tang, and Dingyi Fang. 2019. Tagtag: Material Sensing with Commodity RFID. In *Proceedings of the 17th Conference on Embedded Networked Sensor Systems* (New York, New York) *(SenSys '19)*. Association for Computing Machinery, New York, NY, USA, 338–350. https://doi.org/10.1145/3356250.3360027

[66] Shichao Yue and Dina Katabi. 2019. Liquid testing with your smartphone. In *Proceedings of the 17th Annual International Conference on Mobile Systems, Applications, and Services*. 275–286.